7-11-2018

Search for the Neutron Decay $n \rightarrow X+\gamma$, Where X is a Dark Matter Particle

Z. Tang
Los Alamos National Laboratory

M. Blatnik
California Institute of Technology

L. J. Broussard
Oak Ridge National Laboratory

J. H. Choi
North Carolina State University

S. M. Clayton
Los Alamos National Laboratory

See next page for additional authors

Search for the Neutron Decay $n \to X + \gamma$, Where X is a Dark Matter Particle

Z. Tang,[1] M. Blatnik,[2] L. J. Broussard,[3] J. H. Choi,[4] S. M. Clayton,[1] C. Cude-Woods,[1,4] S. Currie,[1] D. E. Fellers,[1] E. M. Fries,[2] P. Geltenbort,[5] F. Gonzalez,[6] K. P. Hickerson,[2] T. M. Ito,[1] C.-Y. Liu,[6] S. W. T. MacDonald,[1] M. Makela,[1] C. L. Morris,[1] C. M. O'Shaughnessy,[1] R. W. Pattie, Jr.,[1] B. Plaster,[7] D. J. Salvat,[8] A. Saunders,[1] Z. Wang,[1] A. R. Young,[1,4] and B. A. Zeck[1,4]

[1]*Los Alamos National Laboratory, Los Alamos, New Mexico 87545, USA*
[2]*Kellogg Radiation Laboratory, California Institute of Technology, Pasadena, California 91125, USA*
[3]*Oak Ridge National Laboratory, Oak Ridge, Tennessee 37831, USA*
[4]*North Carolina State University, Raleigh, North Carolina 27695, USA*
[5]*Institut Laue-Langevin, Grenoble 38000, France*
[6]*Department of Physics, Indiana University, Bloomington, Indiana 47408, USA*
[7]*University of Kentucky, Lexington, Kentucky 40506, USA*
[8]*University of Washington, Seattle, Washington 98195-1560, USA*

(Received 5 February 2018; revised manuscript received 1 May 2018; published 11 July 2018)

Fornal and Grinstein recently proposed that the discrepancy between two different methods of neutron lifetime measurements, the beam and bottle methods, can be explained by a previously unobserved dark matter decay mode, $n \to X + \gamma$. We perform a search for this decay mode over the allowed range of energies of the monoenergetic γ ray for X to be dark matter. A Compton-suppressed high-purity germanium detector is used to identify γ rays from neutron decay in a nickel-phosphorous-coated stainless-steel bottle. A combination of Monte Carlo and radioactive source calibrations is used to determine the absolute efficiency for detecting γ rays arising from the dark matter decay mode. We exclude the possibility of a sufficiently strong branch to explain the lifetime discrepancy with 97% confidence.

DOI: 10.1103/PhysRevLett.121.022505

There is nearly a five-standard-deviation disagreement [1,2] between measurements of the rate of neutron decay producing protons measured in cold neutron beam experiments [3–5] (888.0 ± 2.0 s) and free neutron lifetime in bottle experiments [6–8] (878.1 ± 0.5 s). The cold neutron beam method consists of counting the number of protons emitted from neutron β decay in a well-characterized neutron beam, and the bottle experiments measure the number of ultracold neutrons (UCNs) that remain inside a trap after a certain storage time. A longer lifetime from the beam measurements could point to the existence of possible other decay modes of the neutron where a proton is not produced. Serebrov has suggested that the discrepancy could be due to neutrons oscillating into mirror neutrons [9,10]. Recently, Fornal and Grinstein suggested in Ref. [11] that the neutron lifetime discrepancy can be explained if the neutron were to decay into a γ ray and a dark matter particle, X. The γ ray has an allowable energy range of 782 to 1664 keV, where it is bounded from above by the stability of ^{9}Be and bounded from below by requiring X to be stable.

Here, we report the results of a search for γ rays arising from UCNs decaying inside a nickel-phosphorous-coated [12], 560 l stainless-steel bottle. The bottle is filled with UCNs from the Los Alamos UCN facility [13] parasitically during the running of the UCN τ experiment [7], with the source operated in production mode. The γ rays are detected in a lead shielded, Compton-scattering-suppressed 140% high-purity germanium (HPGe) detector (Fig. 1). The Compton-scattering suppression is achieved by an anticoincidence with an annular bismuth germinate (BGO) detector surrounding the HPGe detector. The Compton suppression reduced the background in the low energy part of the spectrum by a factor of 1.7. A gate valve placed upstream controlled the loading of UCNs into the bottle. The background γ rates were measured with the UCNs in production mode and the gate valve closed. This resulted in a factor of 4 reduction in the continuum background in the region of interest (ROI).

The energy calibration of the HPGe spectrum was obtained from a linear fit to 13γ-ray lines from sources, natural backgrounds, and prominent neutron capture lines on ^{58}Ni, ^{56}Fe, and ^{35}Cl. The UCN induced γ-ray spectrum was then constructed by subtracting the background spectrum (gate valve closed) from the foreground spectrum (gate valve open). The results of this subtraction are shown in Fig. 2. The peaks in the spectrum are dominated by neutron capture lines on the Ni-P surface and in the stainless-steel bulk of the storage vessel. The bulk neutron capture is due to UCN upscattering on the surface of the coating and subsequent capture in the vessel wall. We have identified 22 prompt γ lines from neutron capture on ^{35}Cl,

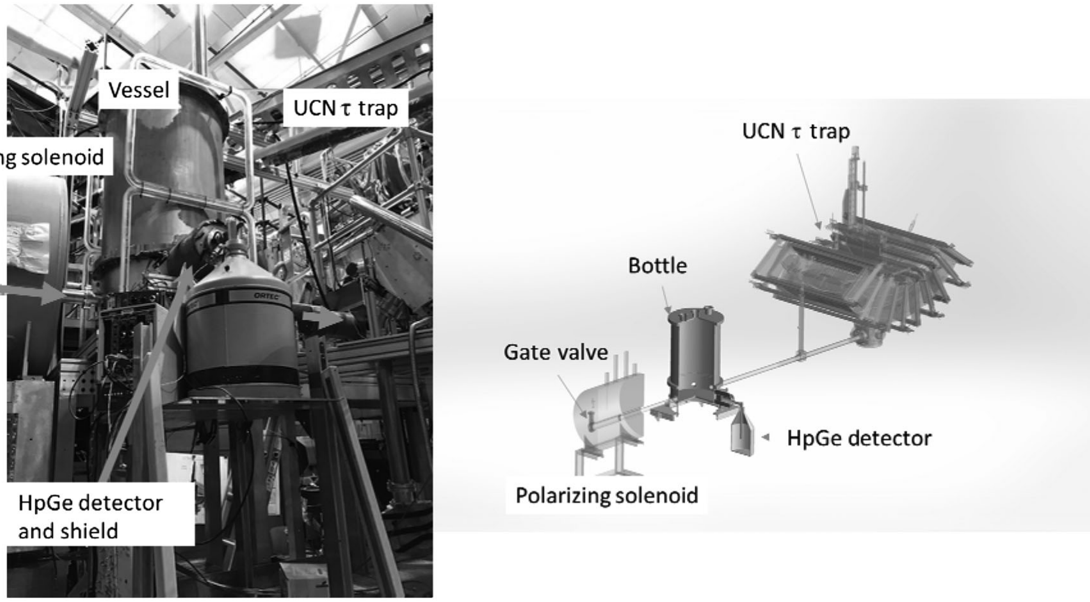

FIG. 1. The UCN bottle is installed in the existing beam line, and a HPGe detector is placed next to the outer wall of the vessel. The UCN gate valve is located upstream of the polarizing solenoid magnet. On the left is a photograph of our setup and on the right is a schematic.

^{50}Cr, ^{52}Cr, ^{53}Cr, ^{56}Fe, ^{58}Ni, ^{60}Ni, ^{62}Ni, ^{63}Ni, and ^{64}Ni in the ROI. There were also two lines present from the β delayed γ rays from ^{24}Na and ^{56}Mn. Nickel is present both in the coating material and in the bulk stainless steel, which also contains iron, chromium, and manganese. Chlorine is used in surface preparation during the nickel phosphorus coating process. Multiple lines outside of the ROI were also identified for chlorine, iron, chromium, and manganese, which helped the isotope identification process. ^{24}Na is produced in the biological shielding stack, and it is present in both the foreground and background measurements. However, because of its long half-life (14.96 h) and the sequential order of the foreground and background measurements, the background subtraction produced a small negative peak.

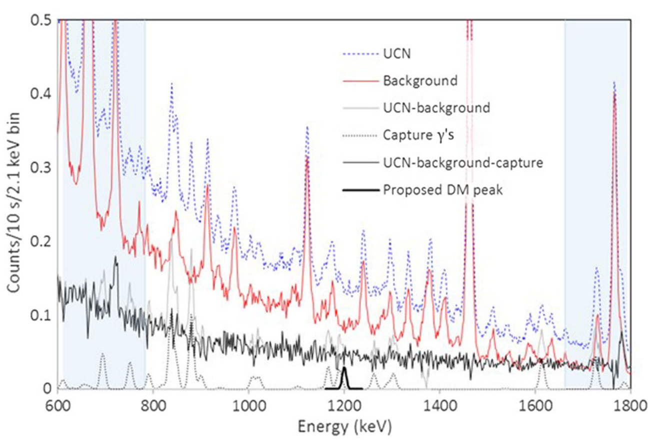

FIG. 2. Measured and simulated spectra in the ROI (white background). The blue and red lines show the Compton-scattering-suppressed spectra for the measurement with UCN and background measurement, respectively. The dotted line shows the simulated spectra from UCN capture and related γ rays. The grey and thin black curves show the net UCN signal and the net signal after capture γ subtraction, respectively. The peak plotted with a thick black line centered at 1200 keV shows an example of the size of the proposed dark matter (DM) decay that would be needed to explain the anomaly.

The experiment was modeled using GEANT4 [14]. The detector-efficiency–solid-angle product was measured using the 1333 keV γ line from a calibrated ^{60}Co source. The simulation reproduced the calibration measurements to within 5% for all points on a vertical scan through the UCN bottle with no adjustable parameters, using the known detector configuration and experiment geometry. The absolute predicted and measured efficiency–solid-angle product at 1333 keV agreed 5%. This allowed the strengths of the γ lines in the allowed region to be computed by normalizing to peaks from the same isotope outside of the allowed region using the relative peak strengths given in Ref. [15], after correcting for the energy dependence of the detector efficiency given by the GEANT4 calculation. This procedure accounts for the unknown capture-production rates for each isotope that produces γ rays in the allowed region experimentally, using only information from outside of the allowed energy region. The normalization had a single global scaling factor and a single factor to normalize all lines from each isotope after correcting for detector efficiency. The results are given in Table I and Fig. 2.

The strength of each peak inside the ROI was calibrated using the peaks from the same isotope outside of the ROI [15]. A list of the lines, origin, and normalization subtracted in the ROI is given in Table I. A GEANT4 [16] simulation

TABLE I. List of origin, strength, and normalization for all of the lines subtracted in the ROI. When two lines are listed in the normalization column, both were used to obtain the normalization and their summed strength is given.

			Normalization					Normalization	
Isotope	Energy (keV)	Strength (counts/10 s)	Energy (keV)	Strength (counts/10 s)	Isotope	Energy (keV)	Strength (counts/10 s)	Energy (keV)	Strength (counts/10 s)
^{35}Cl	788	0.108	6110 + 7414	0.058	^{64}Ni	1107	0.002	6034.8	0.013
^{60}Ni	817	0.030	7820	0.221	^{50}Cr	1149	0.022	1899	0.068
^{53}Cr	835	1.254	2239	0.110	^{35}Cl	1165	0.159	6110 + 7414	0.058
^{62}Ni	846	0.023	6838	0.327	^{60}Ni	1185	0.036	7820	0.221
^{56}Mn	846	0.204	1810	0.040	^{58}Ni	1189	0.124	8534	0.431
^{58}Ni	878	0.587	8534	0.431	^{56}Fe	1261	0.122	7631	0.390
^{50}Cr	888	0.017	1899	0.068	^{52}Cr	1289	0.045	7939 + 7940	0.059
^{56}Fe	898	0.105	7631	0.390	^{58}Ni	1301	0.119	8534	0.431
^{60}Ni	939	0.012	7820	0.221	^{64}Ni	1346	0.001	6034.8	0.013
^{52}Cr	1006	0.093	7939 + 7940	0.059	^{24}Na	1369	−0.462	2754	−0.310
^{56}Fe	1019	0.092	7631	0.390	^{50}Cr	1537	0.012	1899	0.068
^{60}Ni	1100	0.019	7820	0.221	^{56}Fe	1613	0.232	7631	0.390

was used to obtain the energy dependence of the detector. All detector components, including the lead, BGO, and entrance windows, were included in the GEANT4 calculations. This simulation placed a source at the center of the storage volume and included the wall and the detector windows. A peak with a 4.2 keV Gaussian width (the detector resolution) and a normalized peak strength including the relative peak strengths and detector efficiency was generated for each peak inside the ROI, and the sum of all of the peaks was subtracted to obtain the thin black curve in Fig. 2.

To determine the rate of decay into this proposed channel, one needs to know the number of UCNs inside the storage volume. The UCN density inside this storage volume was measured using the vanadium activation method [17,18]. A 1.0 cm diameter foil was mounted on the inside of the wall of the vessel, near the detector. Because of the negative Fermi potential of the ^{51}V, 84% of the UCNs that intercept the foil are absorbed and produce ^{52}V, and a correction is made for neutrons that are upscattered or reflected. Neutron capture on ^{51}V produces ^{52}V, which has a β decay half-life of 3.74 min, and a 1434 keV γ is produced along with the β decay 100% of the time. This γ ray is then detected in the HPGe detector. The efficiency of the germanium detector was normalized by using a ^{60}Co source of known activity (9.3 ± 0.9 kBq) that was placed on top of the ^{51}V foil, and a rate of 1333 keV γ was measured. This accounted for solid-angle and detector efficiency and γ-ray attenuation in the vessel walls. The results were cross calibrated to the measurement by normalizing using upstream ^{10}B/ZnS UCN monitor detectors [19]. The average UCN density at beam height in the storage volume for the foreground measurement was $\rho_0 = 9.5 \pm 1.3$ UCN/cm^3, where the uncertainty is dominated by the corrections to the ^{51}V capture fraction as in Ref. [17].

The Ge detector acceptance for γ rays for each γ emission position inside the UCN storage vessel was measured by scanning the storage volume with the calibrated ^{60}Co source using the 1333 keV line. The 1333 line was used for normalizations because of the small amount of Compton background from the lines above it. First, the source was scanned along a line through the center of the detector. This was fitted with the function $a/(z - z_0)^2$, where z was measured from the cylindrical center of the volume. The constants a and $z0$ were fitted free parameters. This determined an effective center of the detector relative to the center of the storage vessel. Next, a 2D counting rate scan was made in two axes, the axis of the cylinder (y) and an axis normal to z and y. The experimental acceptance measurements are in good agreement (within 5%) with GEANT4 simulations of our detector geometry. After being normalized to the activity of the source, these data were fitted with a function:

$$R(x, y, z) = \frac{A}{r^2} e^{-(\theta^2/2\theta_0^2)}, \tag{1}$$

where $\theta_0 = \arctan(\sqrt{x^2+y^2}/r)$ and $r = \sqrt{x^2+y^2+(z-z_0)^2}$.

The acceptance for γ rays, A, from neutron decay was obtained by integrating this acceptance over the neutron density, assuming a $dN/dv \propto v^2$ distribution, where v is the neutron velocity and N is the neutron density, and accounting for the gravitational distribution of the density [20]:

$$\begin{aligned} \rho(x, y, z) &= \rho_0 y < y_{\rm beam} \\ &= \rho_0 \sqrt{\frac{v_{\rm max}^2 - 2gy}{v_{\rm max}^2}} y_{\rm beam} < y < \frac{v_{\rm max}^2}{2g}, \\ A &= \int_V R(x, y, z)\rho(x, y, z) dV, \end{aligned} \tag{2}$$

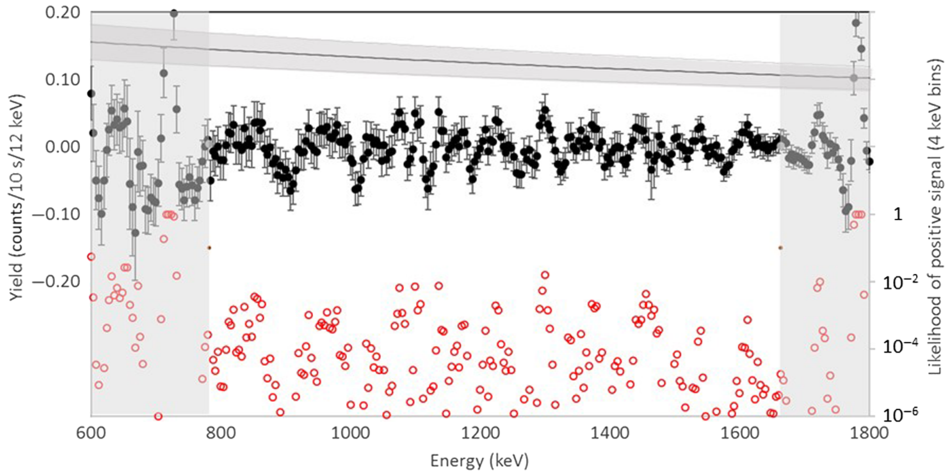

FIG. 3. The data (solid circles) plotted are the sum of counts in a 12 keV (~3 Gaussian peak widths) window above a piecewise fitted background across the ROI. The integration region is centered in a 100 keV wide fitting window, and it is performed in 4 keV steps. The unshaded center of the plot is the ROI. The predicted signal (solid line and shaded region) accounts for the energy dependent photopeak efficiency predicted by GEANT4 [16]. The open circles show the likelihood of the predicted signal in each overlapping bin.

where $\rho(x, y, z)$ is the UCN density as a function of position, $v_{\max}$ is the maximum UCN velocity, g is the acceleration due to gravity, and the integral is over the volume of the vessel. A $v^2 dv$ velocity distribution up to a maximum velocity of 600 cm/s (given by the Fermi potential of upstream stainless-steel guides [20]) is used to determine the height dependence of ρ.

The volume integrated detector sensitivity is 88 ± 9 counts/(decay/cm^3). The branching ratio for UCN decay into dark matter needed to explain the difference in the beam and bottle lifetimes is 1.3%, so the decay rate is 1.2×10^{-5} s^{-1}. The measured density gives an expected rate of 11.9 ± 1.2 mHz, or 0.12 counts/10 s for a peak at 1333 keV. The uncertainty is taken to be the uncertainty in the source activity.

In order to estimate the likelihood of a peak with the predicted signal strength, we have fitted a linear background to 100 keV wide segments of the spectrum and integrated the area above the background in a 12 keV wide region (~3 Gaussian σ peak widths) centered in the segment, to obtain the peak yield, Y_i. The peak region was excluded from the background fit. This procedure was repeated in 4 keV steps across the spectrum for each bin i. The uncertainties, ΔY_i, were calculated assuming Poisson statistics for the foreground and background spectra. The number of standard deviations (x) between each yield, Y_i, and the predicted signal was calculated as $x_{i=}\sqrt{(Y_i - P_i)^2/(\Delta Y_i^2 + \Delta P_i^2)}$, where P_i is the predicted signal and ΔP_i is its uncertainty, obtained by adding the uncertainties in the UCN density and acceptance in quadrature. The likelihood for each i is given by the cumulative normal distribution function. Summing the likelihood over all of the 4 keV wide bins in the ROI and dividing by 3, to account for the 12 keV wide integration window, accounts for the unknown location of a peak [21] (the so-called look elsewhere effect) and excludes the presence of a monoenergetic γ ray in the entire ROI with a total confidence limit of 97%. The largest contributor is the fluctuation at 1130 keV, with a probability of 1.6%.

In Fig. 3, two peaks at 720 and 1779 keV are also shown to demonstrate the sensitivity of our analysis, even though they are outside of the ROI. The 720 keV peak could be due to the decay of ^{10}C, which is a spallation product produced inside the biological shielding stack. The 1779 keV peak is due to the γ ray generated from the β decay of ^{28}Al, which was formed by neutron capture on ^{27}Al. The overlap between adjacent bins can be observed in the saturated likelihood for these peaks.

In summary, we have used the Los Alamos UCN source [13] to search for monoenergetic γ rays from neutron decay to dark matter, a solution recently proposed to explain the difference between beam and bottle neutron lifetime results [11]. Our measurements exclude this possible explanation [11] with 97% confidence.

This work was supported by the Los Alamos Laboratory Directed Research and Development (LDRD) office (Grant No. 20140568DR), the LDRD Program of Oak Ridge National Laboratory, managed by UT-Battelle, Limited Liability Corporation (LLC) (Grant No. 8215), the National Science Foundation (Grants No. 130692, No. 1307426, No. 161454, No. 1506459, and No. 1553861), the Indiana University (IU) Center for Space Time Symmetries (IUCSS), and United States Department of Energy (U.S. DOE) Low Energy Nuclear Physics (Grants No. DE-FG02-97ER41042, No. DE-SC0014622, and No. DE-AC05-00OR22725). The authors would like to thank the staff of Los Alamos Neutron Science Center (LANSCE) for their diligent efforts to develop the diagnostics and new techniques required to provide the proton beam for this experiment.

[1] F. E. Wietfeldt, *Proceedings of the 8th International Workshop on the CKM Unitarity Triangle (CKM 2014), Vienna, Austria, 2014* (to be published).
[2] G. L. Greene and P. Geltenbort, Sci. Am. **314**, No. 4, 36 (2016).
[3] J. Byrne *et al.*, Phys. Rev. Lett. **65**, 289 (1990).
[4] A. T. Yue, M. S. Dewey, D. M. Gilliam, G. L. Greene, A. B. Laptev, J. S. Nico, W. M. Snow, and F. E. Wietfeldt, Phys. Rev. Lett. **111**, 222501 (2013).
[5] J. Byrne, P. Dawber, C. Habeck, S. Smidt, J. Spain, and A. Williams, Europhys. Lett. **33**, 187 (1996).
[6] A. P. Serebrov *et al.*, Phys. Rev. C **78**, 035505 (2008).
[7] C. L. Morris *et al.*, Rev. Sci. Instrum. **88**, 053508 (2017).
[8] R. W. Pattie, Jr. *et al.*, arXiv:1707.01817.
[9] A. Serebrov *et al.*, Phys. Lett. B **663**, 181 (2008).
[10] Z. Berezhiani and L. Bento, Phys. Rev. Lett. **96**, 081801 (2006).
[11] B. Fornal and B. Grinstein, Phys. Rev. Lett. **120**, 191801 (2018).
[12] R. W. Pattie, Jr. *et al.*, Nucl. Instrum. Methods Phys. Res., Sect. A **872**, 64 (2017).
[13] T. M. Ito *et al.*, Phys. Rev. C **97**, 012501(R) (2018).
[14] S. Agostinelli *et al.*, Nucl. Instrum. Methods Phys. Res., Sect. A **506**, 250 (2003).
[15] Thermal neutron capture γ's (CapGam), https://www-nds.iaea.org/capgam/index.htmlx (1 February 2018).
[16] J. Allison *et al.*, Nucl. Instrum. Methods Phys. Res., Sect. A **835**, 186 (2016).
[17] A. Saunders *et al.*, Rev. Sci. Instrum. **84**, 013304 (2013).
[18] A. Frei, K. Schreckenbach, B. Franke, F. Hartmann, T. Huber, R. Picker, S. Paul, and P. Geltenbort, Nucl. Instrum. Methods Phys. Res., Sect. A **612**, 349 (2010).
[19] Z. Wang *et al.*, Nucl. Instrum. Methods Phys. Res., Sect. A **798**, 30 (2015).
[20] R. Golub, D. Richardson, and S. K. Lamoreaux, *Ultra-Cold Neutrons* (CRC Press, Boca Raton, 1991).
[21] L. Lyons, Ann. Appl. Stat. **2**, 887 (2008).